AIAA JOURNAL
Vol. 33, No. 7, July 1995

Unstructured Grid Simulations of Spatially Evolving Supersonic Shear Layers

Choong K. Oh* and Eric Loth†
University of Illinois at Urbana–Champaign, Urbana, Illinois 61801

This research employed an adaptive unstructured finite element grid with a nonlinear monotonic scheme to undertake high-resolution inviscid eddy simulations of spatially evolving supersonic free shear layers. The objectives were to both improve physical understanding and evaluate the simulation fidelity by direct comparisons with detailed experimental measurements. With a physically consistent perturbation model, the compressibility effects on the nature of the shear layer were investigated by testing three different convective Mach numbers, 0.35, 0.45, and 0.7, nonetheless holding velocity and density ratios fixed. Reduction in eddy coherency as compressibility increased was found to be related to modifications in the merging process (slapping vs rotational merges). Turbulence statistics of velocity and mixture fraction exhibited reductions in the peak values of turbulent intensities of transverse velocity and passive scalar as convective Mach number increases, whereas turbulent intensity of streamwise velocity peak values remain constant. In addition, a triple inflection point profile for the mean mixture fraction distribution and a secondary peak for the mixture fraction distribution were found to reduce in intensity as convective Mach number increases. The initial condition sensitivity was also found to be greater at higher convective Mach number due to the lack of large-scale structure development. In general, the results compared well with experiments and were verified with grid resolution studies; but the lack of three-dimensional modes indicated a profound limitation.

Introduction

THE simple flowfield of a planar supersonic shear layer is a generic condition of fundamental importance arising in numerous natural phenomena and practical devices, such as scramjet engines, rocket plumes, separated base flows, thermal sprays, chemical lasers, etc. Therefore, an understanding of the behavior of this flow is essential to predicting compressible turbulence and to setting criteria for the control of mixing in supersonic flows.

Experimental Investigations

Incompressible turbulent free shear layer dynamics have been found to be primarily composed of two-dimensional interactions between neighboring large-scale vortical structures for which sequential mergings of these vortices provide the primary mechanism for the growth rate of the layer in the downstream direction.[1,2] The resulting entrainment, which includes the rate of ingestion of nonturbulent unmixed fluid into the turbulent region, has been referred to as induction, whereas molecular mixing, referred to as infusion, is controlled by the diffusion process which occurs on the viscous scales for a Schmidt number of unity.[3] Roshko[1] noted the self-similarity of the large-scale structures and the important effects of Reynolds number experimentally appear only indirectly through the initial shear layer conditions and not through direct action of viscosity on the developing turbulent structures. This is consistent with results by Ragab and Wu,[4] who showed that the linear instability of typical shear layer profiles was essentially unchanged for Reynolds numbers above 1000. Thus, the essentially inviscid interaction between neighboring large-scale eddies leads to entrainment of the unmixed fluids into the shear layer.

However, the viscous effects also play an important role in determining the laminar or turbulent condition of the initial splitter plate boundary layers. The downstream development of incompressible mixing layers is known to be sensitive to the state of the splitter plate boundary layers, even far downstream: up to 1000 momentum thicknesses (θ) downstream as shown by Bradshaw[5] and up to 2800 θ as shown by Browand and Latigo.[6] A mixing layer with a laminar boundary-layer inflow condition grows more slowly and with a different turbulence evolution as compared to a turbulent boundary-layer condition for approximately the first 100 momentum thicknesses but then overtakes it by 200–300 θ (Ref. 6). The initial unsteadiness and randomness stemming from a turbulent boundary layer as compared to the more coherent but slower development of vortices stemming from a laminar boundary layer may be the primary reason for this difference. This explanation is supported by the streamwise velocity fluctuation measurements of incompressible mixing layers.

Evidence of the reduced mixing encountered in supersonic mixing layers as compared to their subsonic counterparts has been well established in the past decade and has been shown to be related to the large-scale structure's lack of coherency and increasing three dimensionality. Spreading rates were found to be reduced by as much as 75% and the reduction was found to be correlated to the convective Mach number (M_c) (Refs. 7 and 8). The convective Mach number of the two streams is defined with respect to a frame of reference traveling with the speed of large-scale structures in the flow and may be derived based on the isentropic deceleration of both the high-speed and low-speed flow to this frame. However, Dimotakis[9] has shown that the isentropic approximation begins to fail for $M_c > 0.5$.

Three-dimensional structures for incompressible shear layers have been observed experimentally[10,11] where the primary Kelvin–Helmholtz spanwise instabilities were noted to perturb the secondary streamwise instabilities which grow into counter-rotating secondary vortices. Goebel and Dutton[12] found experimentally that for increasing compressibility the transverse turbulence intensity and the normalized Reynolds shear stress decreased, similar to the normalized mixing layer growth rate. However, the streamwise and spanwise turbulence intensities and Reynolds shear stress correlation coefficient were found to remain effectively constant with increasing convective Mach number.[13] Flow visualization by Clemens and Mungal[14] detailed the transition from two-dimensional spanwise-oriented structures ($M_c < 0.4$), to oblique structures ($0.4 < M_c < 0.6$), and eventually to

---

Received March 24, 1994; revision received Nov. 18, 1994; accepted for publication Dec. 5, 1994.

*Graduate Research Assistant, Department of Aeronautical and Astronautical Engineering; currently National Research Council Research Associate Fellow, Laboratory of Computational Physics and Fluid Dynamics, Naval Research Laboratory, 4555 Overlook Ave., SW, Washington, DC 20375. Member AIAA.

†Assistant Professor, Department of Aeronautical and Astronautical Engineering. Senior Member AIAA.

fully three-dimensional structures with reduced coherency ($M_c > 0.6$).

Computational Investigations

Most of the research for compressible mixing layer simulations has employed a temporally evolving approach and used a forcing function to initialize the instabilities. Whereas the temporal and spatial linear stability solution have almost exact agreement, the nonlinear evolution indicates almost exact agreement at the beginning for weak instabilities, but as nonlinear interactions occur, significant differences will exist.[15] In addition, a temporal approach is impractical if one wishes to model effects such as asymmetric entrainment, stream selection rule[9] behavior (for which both relative and absolute Mach numbers are important) or complex geometries. However, the spatially evolving approach has the additional difficulties of specifying inflow and outflow boundary conditions and requires typically an order of magnitude more computing time and memory for the same degree of spatial resolution across the mixing layer. This makes high-resolution three-dimensional spatially evolving simulations extraordinarily intensive. The first comprehensive spatially evolving incompressible simulation, which showed comparison with experimental data in terms of turbulent velocity statistics and mixing layer growth rate, was completed by Chien et al.[16] who concluded that the mean flow evolution of shear layers is dominated by two-dimensional inviscid effects. However, there has not been a compressible counterpart study to date. For two-dimensional temporally evolving mixing layer simulations, the reason for the experimentally observed inhibited spreading rate as M_c increased was explained by embedded eddy shocks which suppress vortex formation and growth.[17,18] Sandham and Reynolds[19] as well as Leep et al.[20] simulated a three-dimensional temporally evolving shear layer and noted the importance of three-dimensional modes for $M_c > 0.6$.

Oh[21] summarized excitation models used for previous incompressible and compressible shear layer simulations and found that, in general, amplitudes and frequencies were based on achieving rapid acceleration of pairing rather than trying to model the natural inflow disturbances given by the boundary-layer initial conditions. However, for a simulation technique of a spatially evolving mixing layer which seeks to predict laboratory or design flows, the perturbations at the inlet plane should be based on physical conditions which characterize the flow turbulence, as will be used in the present study.

Inviscid Eddy Simulations

Direct numerical simulation (DNS) can resolve the full range of physical scales of motion without need of any turbulence model, but its application is typically limited to flows with a moderate Reynolds number. However, Reynolds-averaged Navier–Stokes simulations require a turbulence model which must be adjusted to correlate with experiments and have, thus, not always been robust. Higher Reynolds numbers are possible with large eddy simulations (LES), whose basic idea is to apply spatial filter(s) at a length scale Δ and to include a subgrid model for the filtered stress terms, e.g., Smagorinsky model, to relegate the empiricism to just the smallest scales (although dynamic subgrid modeling[22] shows promise in removing this as well). As Δ is decreased for a given flow problem, less modeling is used and accuracy is increased. For very high-Reynolds number flows, if Δ is sufficiently reduced but is still greater than the Kolmogorov scale, the subgrid model influence becomes asymptotically negligible if the flow is not controlled by a laminar sublayer. Such flows include high Reynolds number turbulent free shear layers, jets, wakes, and some sharp corner separated flow regimes for which Reynolds number does not influence the large part of the mean and turbulent field. Flows for which this would not be applicable include those with any boundary-layer influence, e.g., flows separating from curved surfaces or whose Kolmogorov scale mechanisms significantly affect the large-scale features, e.g., combusting flows. Therefore, for a particular class of flows, sufficient convection resolution with neglect of a subgrid model for the stress terms can eliminate adjustable coefficients.[23] This approach, which should be used with caution, is referred to herein as inviscid eddy simulation (IES).

The resulting neglect of a physical or turbulent viscosity for such flows will lead to a build up of high-frequency energy of wavelength Δ, which can render the equations unstable.[24] Flux corrected transport (FCT) is a computationally inexpensive nonlinear monotone method which can efficiently damp out such frequencies with minimal dissipation to the longer wavelength.[25] However, there is no evidence that this scheme combined with truncation terms provides a subgrid model based on a physical principle, i.e., use of other flux limiting schemes are equally valid options for the IES approach as defined herein. Based on the foregoing remarks, there are two primary IES limitations: 1) The filtered turbulence energy and small-scale structures should be of negligible (not just secondary) importance, which should be confirmed with grid resolution studies. 2) It should only be used in flows where Reynolds number effects are not expected to be significant, i.e., bulk transport dominated flows, since it is incapable of predicting such effects. Such an approach, which employs only nonlinear large-scale eddy development to represent the turbulence energy and transport, has been shown to predict mean and turbulent features of free shear layers with more robustness than Reynolds-averaged calculations.[16,20,26] This success is consistent with the fact that shear layer instability, dynamics and entrainment are all essentially a result of the inviscid nonlinear interaction of the large-scale eddy structures. It should be noted that high resolution for LES or IES is critical in order to achieve high fidelity and grid independent results; however, use of unstructured dynamically adaptive triangular elements designed for high resolution in regions of large gradients (where turbulent energy is significant) has not been previously used for LES or IES. Of the two techniques, IES is more straightforward for such an unstructured grid system because of commutation issues.

Objectives

Our objective is to investigate the behavior of spatially evolving high-Reynolds number turbulent supersonic shear layers with a computational technique well suited for extension to more complex geometries, i.e., an unstructured finite element method. Thus, to simulate the high-Reynolds number flowfield, the IES technique is employed using the two-dimensional Euler equations with the addition of numerical viscosity through FCT. Given the substantial Reynolds numbers of practical (experimental) high-speed turbulent shear layers, artificial viscosity renders physical viscosity negligible based on typical computer resolution limitations, and, thus, one can not assign any particular Reynolds number to the flow. However, the general inflow character is established with a physically consistent initial condition, as opposed to arbitrary selection of perturbation frequencies and amplitudes. The neglect of three-dimensional modes as necessitated by computer limitations of such a spatially evolving simulation is a significant concern despite the apparent predominance of the two-dimensional modes of the turbulent free shear layer and will be addressed accordingly in the Results section. In this context, research issues include the role of large-scale structures and their coherency in the supersonic mixing layer, the modification of the turbulent velocity and mixture fraction statistics as a function of compressibility effects, and evaluation of the simulation fidelity with detailed experimental turbulent flow results.

This study is thus specifically unique in that this is the first study to 1) use solution adaptive remeshing capability combined with an unstructured finite element algorithm for an inviscid eddy simulation, 2) evaluate the fidelity of spatially evolving supersonic shear layer simulations based on detailed experimental statistical information, 3) use a physically consistent excitation function determined from measured turbulent energy levels and spectra to provide these natural inflow disturbances, and 4) investigate the compressibility effects on turbulence statistics of both velocity and mixture fraction caused solely by changes in the convective Mach number. These effects have been investigated for constant density, velocity, and pressure ratios for spatially evolving flows.

Numerical Method

Governing Equations

The numerical model used to carry out the inviscid eddy simulations consists of the two-dimensional, time-dependent conservation equations of mass, momentum, energy, and mixture fraction for an inviscid perfect gas, although artificial viscosity is present (see Oh[21] for further details). The inclusion of passive scalar convection in the present study is performed only to represent the qualitative entrainment development and does not accurately describe the degree of mixedness (since the numerical diffusion is much higher than any species physical diffusion).

The present computational scheme combined a second-order two-step Taylor–Galerkin algorithm with a mass diffused low-order scheme to construct the finite element method with flux corrected transport (FEM-FCT).[27] FCT is applied to provide a nonlinear monotonic shock/contact discontinuity capturing scheme which dampens high-frequency oscillations. For the present study, it was found that basing the flux limiter for all equations, including the mixture fraction, on the minimum of density and energy per unit volume yielded the minimum diffusion which still retained monotonicity when applied on an finite element solution adaptive grid composed of unstructured triangular elements.

For the solution adaptive grid methodology, a local error indicator based on the H-2 seminorm[27] was used to determine if a given element needed to be refined, coarsened, or left alone. Many combinations of error variables and two different error indicators were investigated based on the dynamic range of eddy resolution.[21] In general, it was found that the modified error indicator[27] gave the best results when employed with both density and mixture fraction as the indicator variables.

Computational Domain

The computational domain for this study is shown in Fig. 1, where stream 1 is the high-speed side and where boundary conditions based on Euler flow characteristics are given in the diagram. The length and height were fixed at 40 cm and 4.76 cm to match with Goebel and Dutton's experimental test section size.[12] The inflow conditions are located 1 cm downstream of the splitter plate such that they may be prescribed according to experimental measurements at that streamwise location. The upper and lower boundaries of the computational domain are assumed to be hard walls, which are implemented by tangential velocity slip conditions. For outflow boundaries (which occur at about 800θ downstream), free boundary conditions were used for supersonic outflow, and a characteristic boundary condition on pressure was used for any local subsonic outflow conditions.

Table 1 lists the flow conditions which were simulated, where P, M, T_t, U, and ρ are pressure, Mach number, total temperature, freestream velocity, and density of the two streams, respectively and where δ and θ refer to the boundary-layer thickness and momentum thickness for the two boundary layers. Each simulation requires approximately 6 CPU h and 20 Mwords on a Cray Y-MP. This $M_c = 0.45$ case was chosen because 1) receptivity of the splitter tip was insignificant since both streams were supersonic, 2) it matched experimental flow conditions of Goebel and Dutton,[12] and 3) M_c-0.45 has been shown to exhibit effects of compressibility while still retaining its predominantly two-dimensional character.[14] The two other convective Mach numbers, 0.35 and 0.7, were used to characterize the other two regions of significant compressibility effects[14] but use the same velocity and density ratios across the shear layer as the 0.45 case. The $M_c = 0.35$ case was chosen based on the minimum M_c that still resulted in supersonic mean velocities across the mixing layer, to avoid issues associated with any significant degree of subsonic outflow. $M_c = 0.7$ is beyond the range for which the flowfield is expected to be primarily two dimensional,[14] therefore, this case was only used to investigate the qualitative trends which occur at higher compressibility conditions.

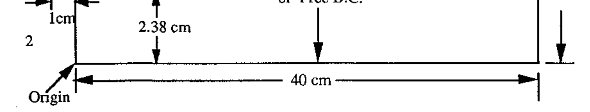

Fig. 1 Physical computational domain and boundary conditions.

Table 1 Flow conditions of three different convective Mach number cases with same velocity (0.57), density (1.56), and Mach number (0.71) ratios

M_c	0.35	0.45	0.7
P (k Pa)	83	49	21
M_1, M_2	1.5, 1.1	1.9, 1.4	2.9, 2.1
T_{t1}, T_{t2} (K)	809, 443	578, 295	385, 171
T_1, T_2 (K)	565, 364	335, 216	141, 91
U_1, U_2 (m/s)		700, 400	
ρ_1, ρ_2 (kg/m^3)		0.51, 0.79	
δ_1, δ_2 (mm)		2.9, 2.5	
θ_1, θ_2 (mm)		0.29, 0.21	

The approximate number of mesh points (20,000) and maximum number of refinement levels (4) for all cases were kept the same, where the refinement/coarsening process was employed every five timesteps. This allowed a minimum spatial frequency (based on two cell lengths) of about 1/22 of the mixing layer thickness at 35 cm downstream with a minimum cell length of 0.03 cm. At this point, the shear layer Reynolds number based on velocity thickness and the freestream velocity difference is 1.2×10^5, consistent with fully developed flow.[12]

Initial Condition Specification

The present study seeks to develop a physically consistent model to provide mean and fluctuating initial conditions which mimic the actual perturbations found for a spatially evolving supersonic shear layer with turbulent boundary layers as the initial condition. This is important since mean distributions of vorticity, perturbation frequencies, and perturbation amplitudes were all shown to significantly influence compressible shear layer development.[21] Turbulent boundary-layer conditions are selected since most engineering applications and laboratory experiments are of this type and since detailed results are available for these conditions. The model to mimic the natural perturbations is based on a variety of frequencies, both due to the turbulent boundary layers and the unresolved mixing layer formation, by imposing oscillations onto the otherwise steady (mean) inflow conditions. These were based on the interpolated rms data from Goebel and Dutton[12] at 1 cm downstream. The inflow boundary data are separated into mean and perturbation profiles as

$$
\begin{aligned}
\rho(x=0, y, t) &= \Psi(y) + \Psi'(y, t)\\
u(x=0, y, t) &= U(y) + U'(y, t)\\
v(x=0, y, t) &= V(y) + V'(y, t)\\
e(x=0, y, t) &= E(y) + E'(y, t)\\
f(x=0, y, t) &= F(y)
\end{aligned}
\tag{1}
$$

where upper case represents initial profiles, and unprimed variables indicate mean functions and primed variables indicate perturbation functions (the mixture fraction is not perturbed because this variable is intended only as a fluid marker). The mean streamwise velocity profile at 1 cm downstream of the splitter plate was specified based on an interpolation curve of the experimental data (Fig. 2a). The perturbation of streamwise velocity from Eq. (1) is expressed for N number of discrete frequencies as

$$
U'(y, t) = \sqrt{2} \sum_{n=1}^{N} \alpha_n U'_{\text{int}}(y) \sin(\omega_n t + \Phi_n) \tag{2a}
$$

where

$$
U'_{\text{int}}(y) = U'_{\max} \operatorname{sech}(8.5y - 22.015) \tag{2b}
$$

and where α_n, ω_n, and ϕ_n are the corresponding perturbation amplitude, frequency, and phase shift, respectively, and the distribution of the interpolated streamwise perturbations U'_{int} is based on a curve fit of the U'_{rms} experimental data at 1 cm downstream of the splitter plate (Fig. 2b). The lack of decay in the experimental fluctuation values below U'_{rms} values of 10 m/s on either side of the shear layer is consistent with the experimental uncertainty of instantaneous velocities (~2%). Similar interpolations were made for $V'_{\rm rms}$ and the experimental correlation coefficient ($R_{u'v'}$) (Ref. 21). The random model then employs both U' and V' experimental mixing layer spectra with the interpolated turbulence quantities. The amplitudes of 13 arbitrarily selected discrete frequencies from the incompressible mixing layer turbulent spectra of Wygnanski and Fiedler[28] were used to span mesh dynamic range (Fig. 3). These frequencies were given random phase angle relationships and then properly scaled[21] to account for the much higher frequencies of the present flow. This scaling was accomplished through normalizing the frequencies with the appropriate local vortex passage frequency (f_n), which was computed using an empirical relationship for vortex spacing given by Koochesfahani and Dimotakis.[29] This allowed a detailed kinetic energy initial condition, rather than one based on perturbations of theoretical harmonics with only the fastest pairing phase shifts.

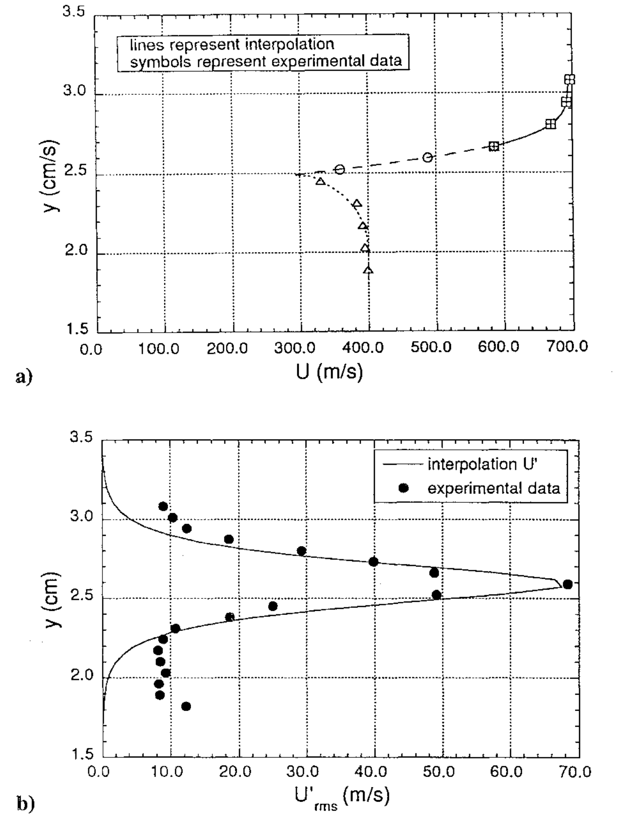

Fig. 2 Empirical curve fits of the compressible shear layer data at $x = 1$ cm: a) mean streamwise velocity and b) $U'_{\rm rms}$.

The expression for the uncorrelated component of the transverse velocity fluctuations $V'_u(y,t)$ is then expressed by

$$V'_u(y,t) = \sqrt{2}\sum_{j=1}^{13}\beta_j V'_{\rm int}(y)\sin(\omega_j t+\Phi_j), \quad \text{where} \quad \sum_{j=1}^{13}\beta_j = 1 \tag{3}$$

where $V'_{\rm int}$ is the interpolated curve fit for the experimental $V'_{\rm rms}$ (Fig. 2b). The correlation coefficient between the streamwise and transverse fluctuation velocities was then employed to obtain the final form of the V' formulation as follows:

$$V'(y,t) = \left[\frac{U'(y,t)}{U'_{\rm int}(y)}R_{u'v'}(y)V'_{\rm int}(y) + (1-|R_{u'v'}(y)|)V'_u(y,t)\right] \tag{4}$$

where $R'_{u'v'}$ is based on the empirical curve fit for Reynolds stress.[21] Density and energy fluctuations were then calculated based on the assumption of constant entropy and mean pressure. The correlation model with random phase shifts is felt to be physically consistent, since it is based on all of the available experimental inflow data including detailed spectra.

Results

Flow Dynamics

Flow evolution was determined from animations and instantaneous Gouraud shaded images of mixture fraction, density, velocity vectors, etc. Typical mixture fraction gray scale distributions at a fully developed state are shown for the three different convective Mach numbers (0.35, 0.45, and 0.7) in Fig. 4. The passive scalar provides a very useful method for viewing and interpreting the simulation data but is only an indication of the large-scale structure coherency and induction entrainment and not of physical diffusion. However, the streakline character of the mixture fraction shows such processes more clearly than the streamline character of the velocity vector field.

The $M_c = 0.35$ case (Fig. 4a) shows Kelvin–Helmholtz instability growth as the shear layer first develops and forms the first distinct vortex at approximately $x = 15$ cm downstream. Afterward, growing eddies evolve through rotational pairing and typically exhibit the round shape of classic incompressible circular eddies. The first eddy of $M_c = 0.45$ case (Fig. 4a) is formed at almost the same position as the $M_c = 0.35$ case, and the eddy sizes for these two cases are very comparable. However, the eddies of the $M_c = 0.70$ case are delayed in initial formation, more elongated into the streamwise direction, and the vortex edges exhibit more corrugation. The large-scale structure shapes of this case appear as multiple striations with an oblique angle and are consistent with previous experimental and computational results.[7,12,13,15,17,26,30] Figure 4d shows the instantaneous mesh refinement levels for $M_c = 0.45$. Outside of the shear layer, the background elements can be seen and inside the shear layer high resolution along braids and edges of vortices are noted.

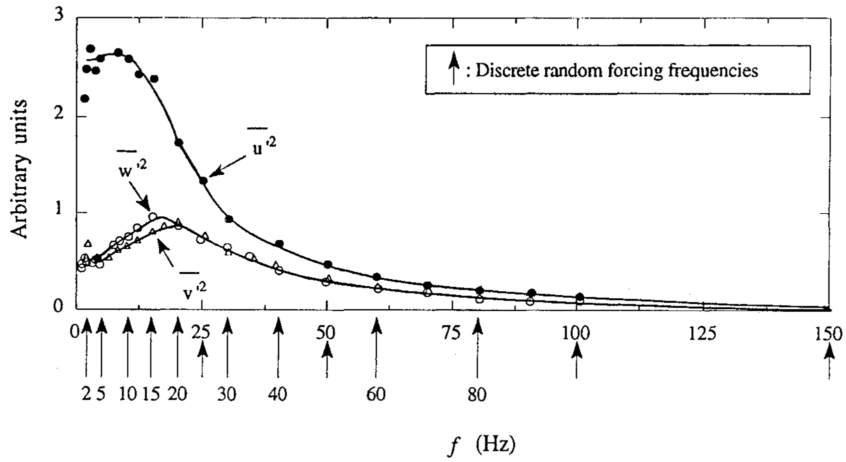

Fig. 3 Incompressible shear layer turbulent energy spectrum from Wygnanski and Fiedler[28] with discrete random forcing frequencies corresponding to vertical arrows which were scaled by matching the most energetic frequency.

Perhaps, the most noteworthy aspect of the flow animations is the different merging processes noted between the three cases. Two types of merging phenomena, i.e., eddies slapping into each other vs their spinning around to form a new one, were noted, as defined by Fig. 5. Slapping first appears for the $M_c = 0.45$ case, and it becomes the predominant merging process for the $M_c = 0.70$ case. This slapping mechanism looks like a wave hitting a beach with structure dissipation. It is presumably found for increasing M_c due to 1) the suppression of perturbations by the supersonic ambient flows as the ratio of gas dynamic forces to vorticity forces increases, and 2) the reduction in pressure signal propagation from the downstream vortex to the upstream vortex (which tells the upstream vortex to move up). What is also important about this modified merging process is that a large portion of the vortex coherency and growth rate is directly lost as a result, based on detailed quantitative vortex tracking statistics.[31] However, three-dimensional interactions (vortex stretching) play an important role in turbulent flows, particularly at the high-convective Mach numbers, which will yield other aspects of merging modification.

Mixing Layer Growth Rates

Figure 6a shows comparison of visualization mixing layer thicknesses based on numerical and experimental schlieren photographs for the $M_c = 0.45$ case along with the experimental result.[12] Although this visualization thickness measurement is subject to numerical diffusion and experimental uncertainty, the present numerical results show reasonable agreement with experimental data. However, the velocity thickness is more dependable than visualization thickness because of its clear definition and statistics.

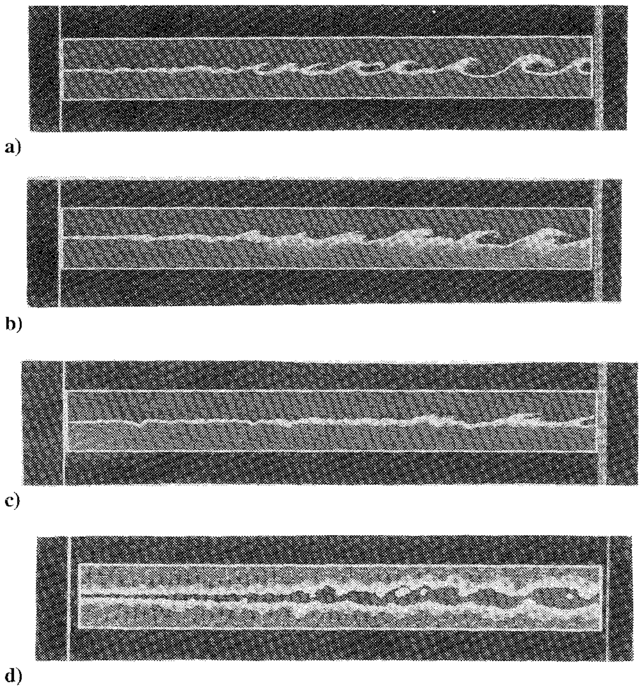

Fig. 4 Mixture fraction shaded contours at a fully developed state for a) M_c = 0.35, b) M_c = 0.45, c) M_c = 0.7, and d) mesh refinement level at fully developed state of M_c = 0.45 case.

Fig. 5 Two different vortex merging processes: a) rotational pairing and b) slapping.

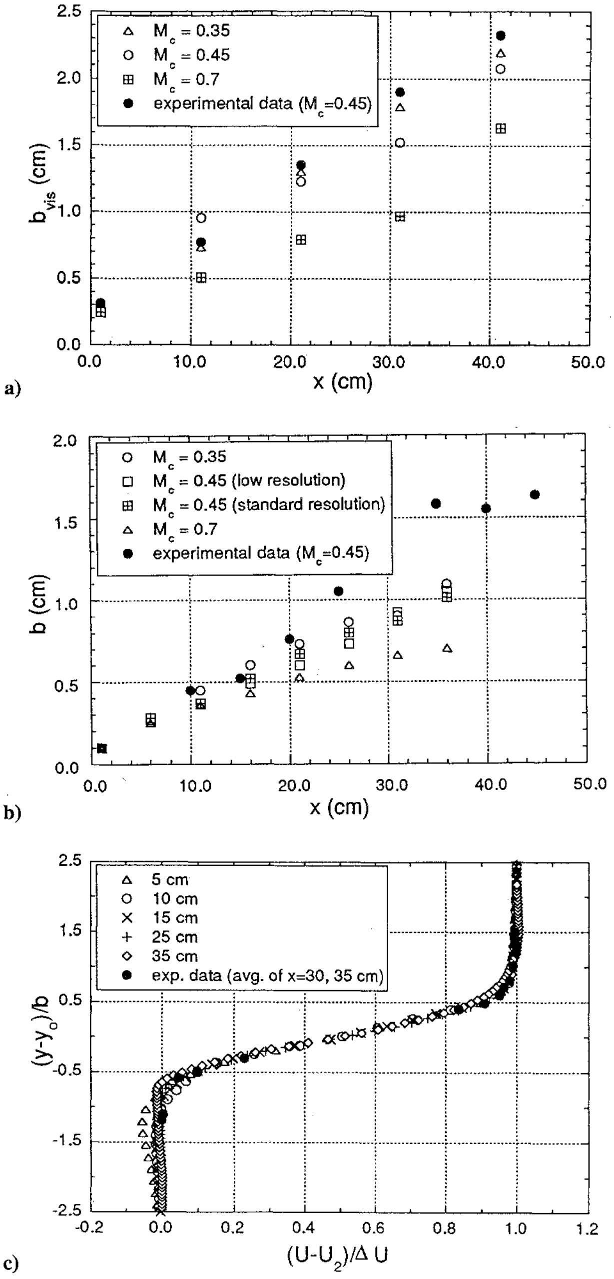

Fig. 6 Mixing layer growth rate based on a) visualization thickness, b) streamwise velocity, and c) normalized mean streamwise velocity for M_c = 0.45.

The mixing layer thickness based on velocity vs streamwise distance is plotted for all three cases along with Goebel and Dutton's data[12] in Fig. 6b. This mean thickness (b) is defined to be the distance between transverse locations where $U = U_1 - 0.1\Delta U$, $U = U_2 + 0.1\Delta U$, and where ΔU is freestream velocity difference. Note all statistics presented in this study were taken after the shear layer had reached a statistically steady state (0.72 ms) and were subsequently averaged over time periods sufficient to remove any significant time dependence (0.95 ms). The flows up to $x = 6$ cm show almost the same growth rate for all three cases, due to the linear regime of instabilities and numerical diffusion, and then differences between the three cases become significant farther downstream in accordance with expected trends (see the Introduction). The interpolated slopes of these growth rates are 0.027, 0.025, and 0.017 as M_c increased, which is consistent with Fig. 4 and similar plots based on visualization thickness. However, the $M_c = 0.45$ case exhibits significant underprediction as compared to experiment after $x = 20$ cm (400θ).

To understand the underprediction, growth rates of two other spatially evolving simulations were evaluated by Oh[21] with a simple empirical formula given by Messersmith.[30] Lele[17] conducted a spatially evolving full Navier–Stokes simulation at M_c of 0.4, and the resulting growth rate of mixing layer vs distance downstream normalized by initial vorticity thickness (δ_{ω_0}) showed reasonable agreement with the empirical growth rate up until $40\delta_{\omega_0}$ downstream; thereafter, significant underprediction occurred. Similar results by Lowery and Reynolds[32] for a two-dimensional incompressible mixing layer show a taper off at approximately $50\delta_{\omega_0}$ downstream, again similar to the $60\delta_{\omega_0}$ taper off downstream distance of the present results. However, Lowery and Reynolds' three-dimensional simulation for the same case showed increased growth rates beyond this distance, significantly above the empirical rate. Recent incompressible temporally evolving shear layer predictions of Moser and Rogers[33] showed the same distinction between two- and three-dimensional flows and was attributed to the presence of both oblique and streamwise vorticity which contributes to additional instability modes and allows for vortex stretching. Such phenomena were observed experimentally by Bernal and Roshko[10] and result in enhancement of the spreading rate. Thus, the growth rate underprediction of the present study is likely caused by the lack of three-dimensional character and is felt to be the most profound limitation of the present study.

A sample plot of mean streamwise velocity profiles is shown in Fig. 6c for $M_c = 0.45$, where the similarity parameter $\eta = (y - y_0)/b$ is used and the velocity was normalized by $(U - U_2)/\Delta U$. Because of significant experimental scatter, the $M_c = 0.45$ experimental results[12] were averaged values over two stations, at $x = 30$ and 35 cm. In general, the mean streamwise velocity profiles for all three convective Mach numbers were very similar and yielded near hyperbolic tangent shapes that matched well with experiment. However, the degree of wake effects due to the splitter tip was more somewhat pronounced as convective Mach number increased.

Turbulent Velocity Statistics

Figures 7–9 are development profiles of streamwise turbulent intensity and transverse turbulent intensity, where σ_U and σ_V are annotations for $U'_{\rm rms}$ and $V'_{\rm rms}$ which were normalized by the freestream velocity difference ΔU. In addition to the comparison with the $M_c = 0.45$ experimental results, the simulation data of the $M_c = 0.70$ case is shown along with a second experimental data set[12] whose convective Mach number is 0.72, but with a significantly different velocity ratio (0.24) and density ratio (1.73) as compared to those of the simulation counterparts (0.58 and 1.56), and a subsonic low-speed stream. Thus, unlike $M_c = 0.45$, the experimental conditions are not the same as the computational conditions, and the data should be viewed for qualitative comparison only.

The $U'_{\rm rms}$ predictions for the three convective Mach numbers are shown in Fig. 7. All three cases exhibit both a primary peak at the centerline as well as secondary shoulders at values of η near 0.7. Whereas the experimental results do not show these secondary peaks, incompressible experiments[36] and DNS[32] do show such peaks. Figure 8 shows an idealized model to explain the secondary peaks at both the high- and low-speed sides. If the vortex shapes are perfect circles, without merging or vertical displacement occurring, the streamwise fluctuation velocities at the vortex edges are accelerated in opposite directions. Therefore, the $U'_{\rm rms}$ would have two secondary peaks corresponding to the upper and lower edges of the vortices. In reality, the compressible eddies are not circular, and their nonlinear interactions yield a complex dispersion which results in a primary peak. However, if large-scale structures have strong coherency, two secondary peaks may still occur. This premise can be extended by arguing that these secondary peaks will be weaker as the mixing layer loses coherency, which occurs as M_c increases (Fig. 4). This is also supported by the $U'_{\rm rms}$ results (Fig. 7) which exhibit weaker secondary peaks as the convective Mach number increases. Their lack of existence in the experimental profile is presumably due to three-dimensional effects and small-scale structures, both of which will cause transverse and spanwise perturbation of the large-scale structures, thus masking the secondary peaks through spatial diffusion and nonlinear interactions. The profiles for all three $U'_{\rm rms}$ cases (Fig. 7) show rapid convergence after $x = 10$ cm downstream. The converged peak values of the three different convective Mach numbers remain constant. This is consistent with the Goebel and Dutton experimental results[12] which indicate $U'_{\rm rms}$ is not strongly affected by compressibility but is contrary to other experimental results of Elliot and Samimy.[34]

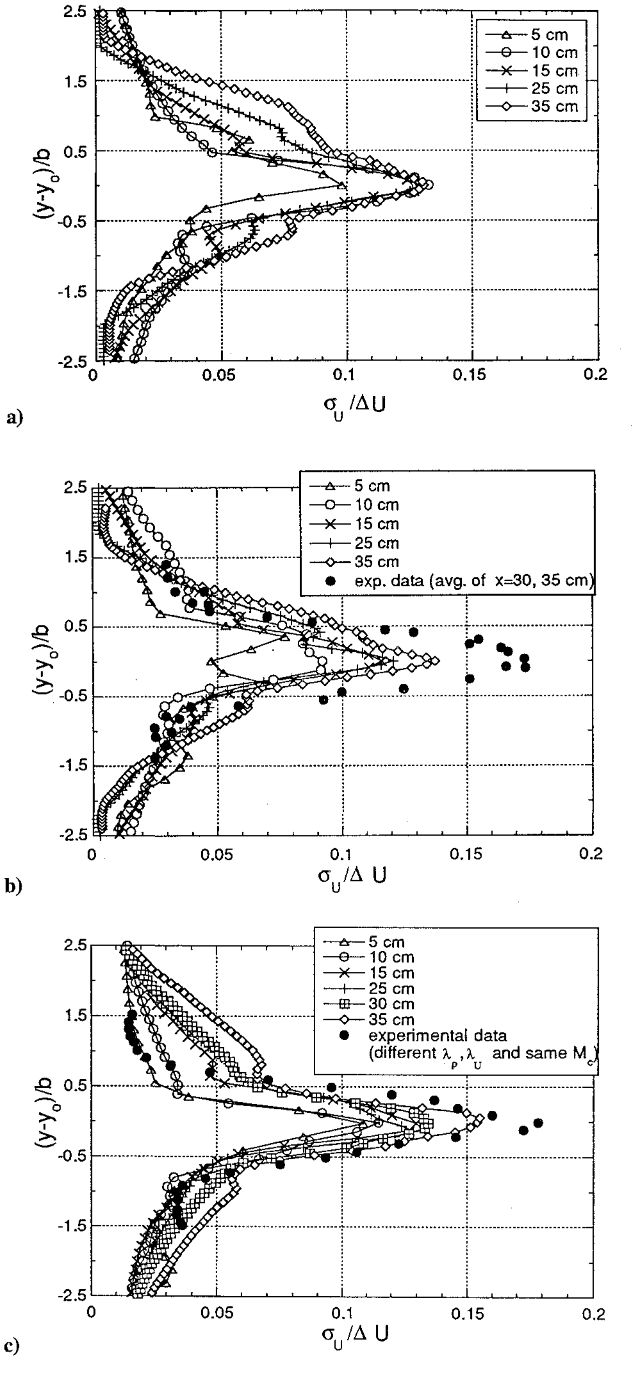

Fig. 7 Normalized streamwise turbulence intensity for a) M_c = 0.35, b) M_c = 0.45, and c) M_c = 0.70.

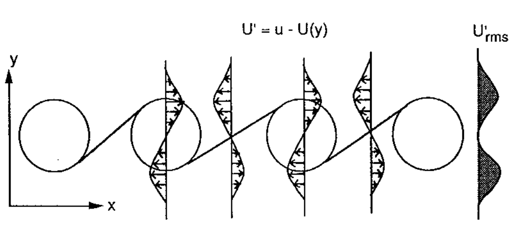

Fig. 8 Streamwise velocity profile at the vortex cores and braids and $U'_{\rm rms}$ profile in the temporally evolving frame of reference.

The $V'_{\rm rms}$ predictions for the three convective Mach numbers are shown in Fig. 9. All three cases exhibit only a primary peak value near the centerline which is consistent with the experimental

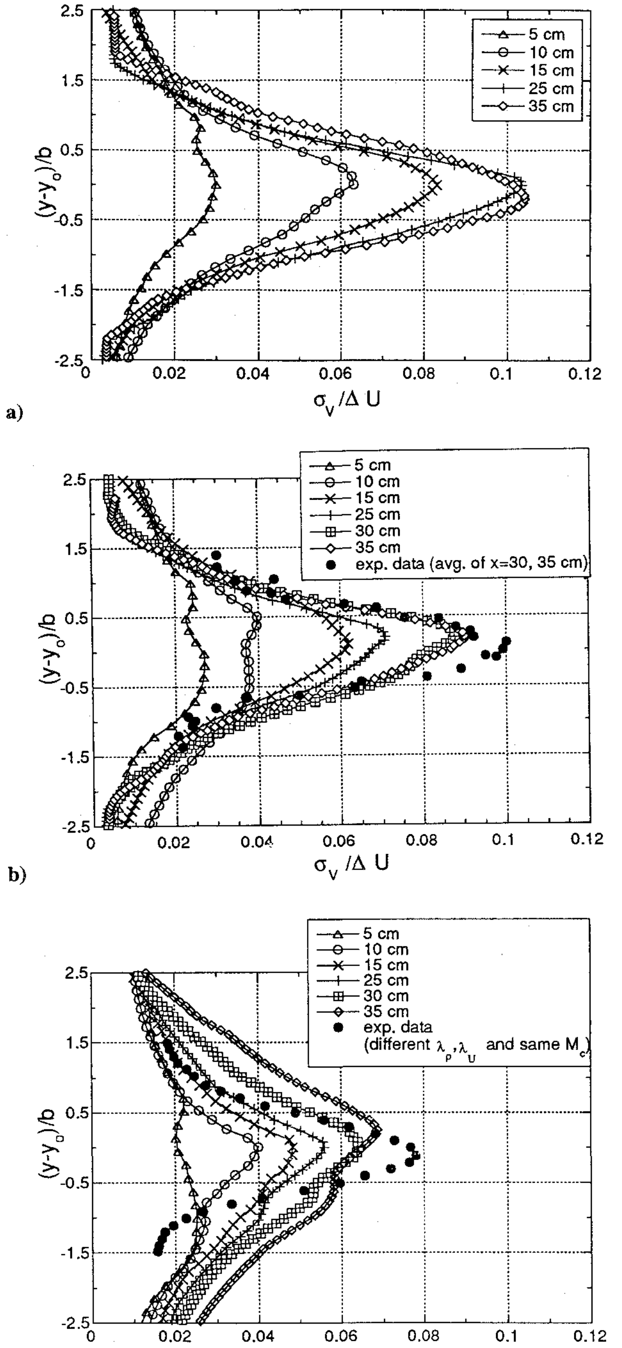

Fig. 9 Normalized transverse turbulence intensity for a) $M_c = 0.35$, b) $M_c = 0.45$, and c) $M_c = 0.70$.

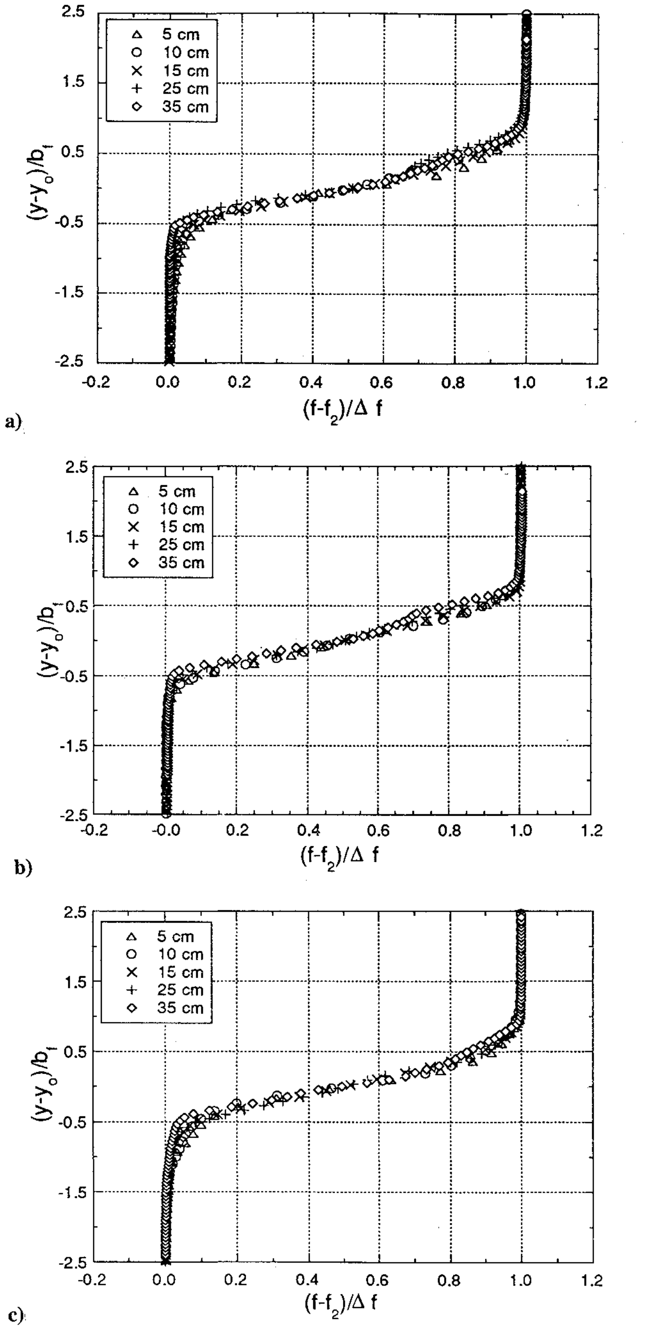

Fig. 10 Normalized mean mixture fraction profiles for a) $M_c = 0.35$, b) $M_c = 0.45$, and c) $M_c = 0.70$.

results.[12] The peak values of the $M_c = 0.35$ and $M_c = 0.45$ cases gradually increase farther downstream and eventually converge after $x = 30$ cm. Their shapes are also well predicted. However, the highest convective Mach number case does not exhibit convergence, and its shape is more diffused, especially at $x = 35$ cm. Since the additional diffusion of $V'_{\rm rms}$ of this case is not due to resolution (all cases used the same grid parameters), it may be related to the additional compressibility above and below the vortex as M_c increases. The $V'_{\rm rms}$ levels at $x = 5$ cm downstream for all cases were found to be much lower compared to their $U'_{\rm rms}$ counterparts. This loss of transverse turbulent kinetic energy (as opposed to streamwise turbulent kinetic energy) is attributed to the lack of coherency of the initial perturbations, which are initially diffused until eddy structures finally form.

The converged peak values of $V'_{\rm rms}$ and Reynolds stress (given in Oh[21]) decrease as the M_c increases, which is consistent with experimental results.[12] This is also consistent with animations which indicated that $V'_{\rm rms}$ was correlated to eddy size and structure coherency.[21] The distribution of the U'–V' correlation coefficient was also found to be reproduced to within 20% of the experimental distribution.[21] In general, spanwise undulations of the shear layer associated with streamwise vorticity can significantly increase the average mixing layer thickness and $U'_{\rm rms}$ since the mean streamwise velocity would correlate with such changes, whereas $V'_{\rm rms}$ is based on a mean transverse velocity of nearly zero throughout the shear layer and would not be as strongly affected by such undulations. This qualitatively explains the comparison with experiment of b, $U'_{\rm rms}$, and $V'_{\rm rms}$. However, it should be kept in mind that three-dimensional perturbations also fundamentally affect the nonlinear pairing and the eddy growth process which may be the more likely reason for the underestimation of velocity thickness.

Mixture Fraction Statistics

For the mixture fraction statistical distributions, a second similarity coordinate is defined by employing the mean mixture fraction profile. Mean mixture fraction profiles (Fig. 10) are shown for all

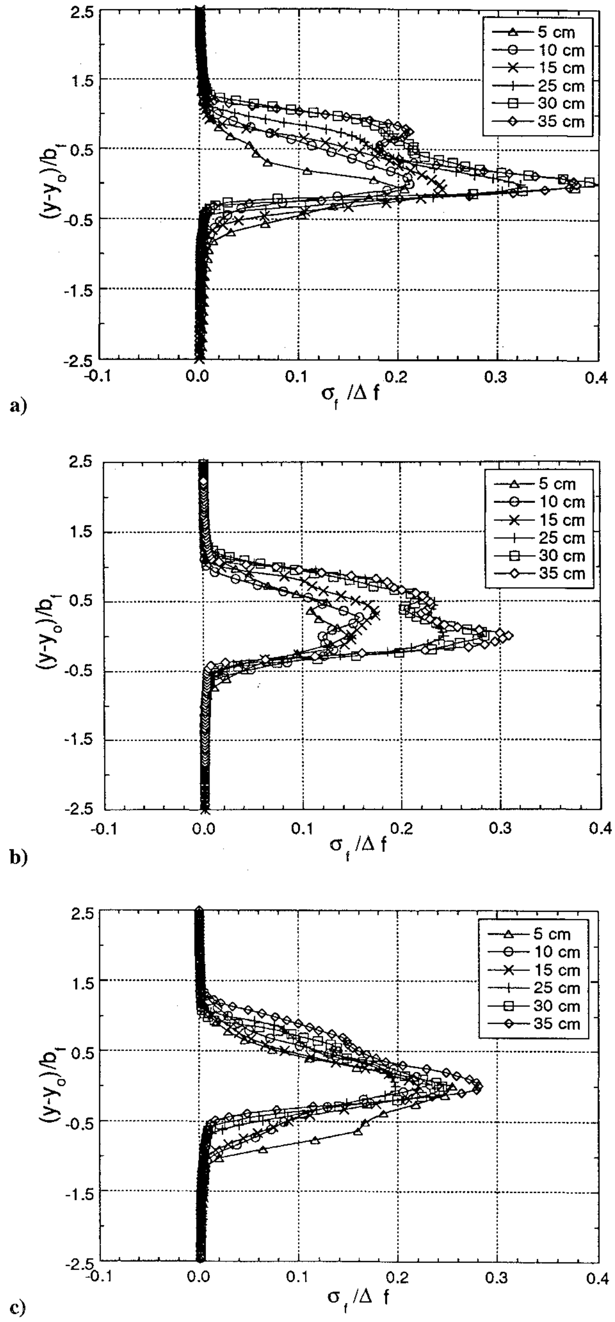

Fig. 11 Normalized mixture fraction fluctuation profiles for a) M_c = 0.35, b) M_c = 0.45, and c) M_c = 0.70.

three cases. These profiles exhibit a subtly different character when compared with the mean streamwise velocity profiles. As can be seen from Fig. 6c, the mean streamwise velocity distribution curve has a single inflection point indicating an ordinary gradient diffusion mechanism for the momentum. In contrast to this, the mean mixture fraction distribution curves have three inflection points. This is consistent with incompressible experimental results[35,36] and a two-dimensional incompressible simulation result of Sandham and Reynolds.[37] However, this triple inflection point has not been reported for compressible flows. Fiedler[36] concluded that this peculiar shape of the curve suggests a transport mechanism largely determined by quasiconvective action due to large vortex motion (bulk convection). These secondary inflection points are reduced in strength as M_c increases, supporting their relationship to large-scale coherent structures.

The mixture fraction fluctuation intensity profiles are shown in Fig. 11 for all three cases. In general, the mixture fraction fluctuation profiles are quite different from the streamwise velocity fluctuation intensity profile due to the presence of a secondary peak, in addition to the primary peak. This secondary peak for cases M_c = 0.35 and 0.45 is consistent with incompressible[35] and compressible[31] experiments and relates to asymmetric entrainment which can only be observed in spatially evolving flows. The present numerical results exaggerate this phenomenon as compared with high-Reynolds number experiments,[31] presumably due to lack of both three-dimensional variations and small-scale features in the simulation.

The primary peak values of f'_{rms} also show a decrease as M_c increases, due to the additional diffusion caused by the lack of eddy coherency. Note that if there were no numerical diffusion, we would always expect a f'_{rms} peak of 0.5. The intensity of the secondary peak in the high-speed side is most pronounced for the low M_c flow and is nearly gone for the high M_c flow. This may be explained by considering the flow evolution. Large-scale structures are known to entrain more from the high-speed side[3]; as coherency increases, so does mixture fraction convolution and, thus, so does intermittency between mixed fluid and entrained ambient fluid, possibly resulting in such a peak.

Grid Resolution Studies

Grid resolution studies were performed to determine solution sensitivity of the compressible shear layer IES predictions. Since the standard resolution runs used approximately 20,000 grid points, low resolution runs were completed by reducing the nodes used to approximately 10,000 by changing the number of refinement levels from four to three. This effectively reduced the cell resolution (Δx) only in the flow regions downstream of 20–40 cm, since a minimum cell size constraint prevented fourth level refinement of the upstream region. The resulting maximum resolution ($b/\Delta x_{\min}$) averaged for the 20–40-cm domain thus went from 27 to 13 as the resolution was relaxed. The mixing growth rate exhibited only small differences between the low and standard resolution runs of the $M_c = 0.45$ case (Fig. 6b). The velocity and mixture fraction statistics of the low resolution and standard resolution runs also exhibited only small differences as well,[21] the most exaggerated of which was the streamwise turbulence intensity profiles (compare Fig. 12 with Fig. 7b). Based on the foregoing statements, it appears that the downstream portion of the shear layer is reasonably grid independent.

A high resolution case, which included approximately 40,000 points, was also performed for $M_c = 0.45$ by only reducing the minimum mesh size from 0.03 cm to 0.015 cm (keeping the same four levels of refinement). The fourth refinement level for the high resolution run penetrates all of the way upstream, whereas the standard resolution run only showed the fourth refinement level from x = 20–40 cm. Thus, this test investigated the flow sensitivity to additional upstream refinement, as opposed to increasing refinement levels. Although it was deemed too expensive to obtain turbulent statistics of the high resolution case, the additional refinement yielded better eddy resolution at x = 5 cm and somewhat larger visualization thickness downstream. This is not surprising since $b/\Delta x_{\min}$ for the

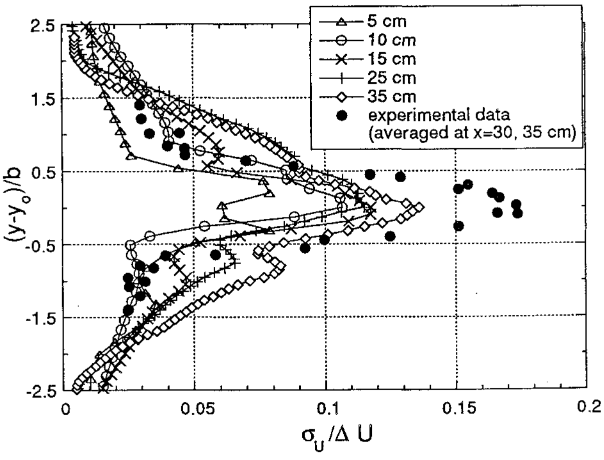

Fig. 12 Normalized streamwise turbulence intensity for a low resolution for M_c = 0.45, compare with Fig. 8b at standard resolution.

standard resolution at this upstream position is only 10, whereas $b/\Delta x_{\min}$ for the high resolution is approximately 20. However, the downstream large-scale dynamics were not significantly affected by this resolution increase. This indicates that a minimum $b/\Delta x_{\min}$ of approximately 20 is necessary to have local grid independence. This is also consistent with the low resolution results and results of Chien et al.[16] which used $b_{\max}/\Delta x_{\min}$ of approximately 34, which is similar to the $b_{\max}/\Delta x_{\min}$ of this study (37). Therefore, one wishes to have this level of resolution ($b/\Delta x_{\min} \geq 20$) throughout the domain.

It is estimated that in some cases storage and CPU requirements are 10–100 times lower for an adaptive grid than for a uniformly fine mesh.[27] But such comparisons have not been made for LES or IES simulations. The measured nodal CPU time for the current solver was 60 μs/node/timestep and the RAM required was 185 words/node for the standard resolution case. This is significantly greater than for an explicit structured grid solver (which does not require a dynamic interdependency matrix) on the same machine, e.g., only 10 μs/node/timestep and 30 words/node. However, we must account for the grid refinement advantages. For example, achieving the standard resolution with a uniformly fine structured grid with the same minimum grid size would take about 210,000 nodes, but require about twice the RAM and twice the CPU time (since the timestep is about the same). In addition, the unstructured grid code should show additional savings as the refinement level is increased and will be more robust and efficient for complex geometries; however, structured grid codes are more easily implemented on massively parallel computers

Conclusions

Supersonic shear layers were modeled with inviscid eddy simulations using a solution adaptive unstructured finite element method. The main difference between the present spatially evolving results and those of temporally evolving shear layers is that the latter can not capture either the asymmetric behaviors noted in the statistics (especially for the mixture fraction) or any effects resulting from the stream selection rule of Dimotakis.[9] If one wishes to robustly compute high-Reynolds number flows such as shear layers and jets which do not have a controlling laminar sublayer, IES represents a practical alternative which allows the description of coherent structure dynamics in both convection and merging. However, it is incapable of predicting Reynolds number effects since it does not include physical viscosity. In addition, attention must be paid to grid resolution, e.g., $b/\Delta x_{\min} \geq 20$ should be preserved locally in order to yield converged grid independent results. For the present IES, physically consistent inflow conditions were obtained by using an experimentally measured mean velocity profile which includes a wake defect and randomly chosen wavelengths based on a measured turbulence spectra and measured initial turbulent kinetic energy levels and mean correlation.

The results show that the two-dimensional merging process was found to vary as a function of M_c, i.e., the rotational vortex pairing process at low M_c converts to a slapping process at high M_c. This slapping process, which results in eddy flattening and oblique angles at higher M_c, reduces the degree of coherency, presumably due to the reduced signal propagation at higher M_c. When compared with experiment, mixing layer widths were predicted reasonably well when based on visual thickness, U'_{rms} or V'_{rms} profiles; but the simulations significantly underpredicted growth rate based on mean velocity, which is attributed to the lack of three-dimensional effects. The converged peak values of V'_{rms} and f'_{rms} are reduced, whereas U'_{rms} peak values remain constant as M_c increases, consistent with experimental results of Goebel and Dutton.[12] The development of the mean and turbulent profiles was found to be more sensitive to initial conditions as M_c increased due to the accompanying reduction in coherency. Mixture fraction statistics exhibit triple inflection points on mean profiles and secondary peaks on the high-speed side of f'_{rms} profiles, caused by the strong presence of coherent structures. The mechanism to produce these peculiar shapes is removed as coherency decreases for increased M_c. However, the most profound limitation of the present study is deemed to be neglect of the three-dimensional effects, which are expected to significantly affect the results.

Acknowledgments

The authors would like to acknowledge the financial support provided by the National Science Foundation under Grant CTS-9010594 with S. P. Traugott as Technical Monitor, and the computer resources provided by the National Center for Supercomputing Applications. We would like to thank J. C. Dutton at University of Illinois at Urbana-Champaign for valuable discussions, R. Löhner at George Mason University for the original code, and J. Lin for aid in video simulation.

References

[1] Roshko, A., "Structure of Turbulent Shear Flows: a New Look," *AIAA Journal*, Vol. 14, No. 10, 1976, pp. 1349–1357.

[2] Winant, C. D., and Browand, F. K., "Vortex Pairing: the Mechanism of Turbulent Mixing-Layer Growth at Moderate Reynolds Number," *Journal of Fluid Mechanics*, Vol. 63, Oct. 1974, pp. 237–255.

[3] Dimotakis, P. E., "Two-Dimensional Shear Layer Entrainment," *AIAA Journal*, Vol. 24, No. 11, 1986, pp. 1791–1796.

[4] Ragab, S. A., and Wu, J. L., "Instabilities of Supersonic Shear Flows," AIAA Paper 90-0712, Jan. 1990.

[5] Bradshaw, P., "The Effect of Initial Conditions on the Development of a Free Shear Layer," *Journal of Fluid Mechanics*, Vol. 26, Sept. 1966, pp. 225–236.

[6] Browand, F. K., and Latigo, B. O., "Growth of the Two-Dimensional Mixing Layer from a Turbulent and Nonturbulent Boundary Layer," *Physics of Fluids A*, Vol. 22, No. 6, 1979, pp. 1011–1019.

[7] Papamoschou, D., and Roshko, A., "The Compressible Turbulent Shear Layer: An Experimental Study," *Journal of Fluid Mechanics*, Vol. 197, Dec. 1988, pp. 453–477.

[8] Bogdanoff, D. W., "Compressibility Effects in Turbulent Shear Layer," *AIAA Journal*, Vol. 21, No. 6, 1983, pp. 926, 927.

[9] Dimotakis, P. E., "Turbulent Free Shear Layer Mixing and Combustion," *High-Speed Flight Propulsion System*, edited by S. N. B. Murthy and E. T. Curran, Vol. 137, Progress in Astronautics and Aeronautics, AIAA, Washington, DC, 1991, pp. 265–340.

[10] Bernal, L. P., and Roshko, A., "Streamwise Vortex Structure in Plane Mixing Layer," *Journal of Fluid Mechanics*, Vol. 170, Sept. 1986, pp. 499–525.

[11] Lasheras, J. C., and Choi, H., "Three-Dimensional Instability of a Plane Free Shear Layer: an Experimental Study of the Formation and Evolution of Streamwise Vortices," *Journal of Fluid Mechanics*, Vol. 189, April 1988, pp. 53–86.

[12] Goebel, S. G., and Dutton, J. C., "An Experimental Investigation of Compressible, Turbulent Mixing Layers," Dept. of Mechanical and Industrial Engineering, Univ. of Illinois at Urbana–Champaign, Technical Rept. UILU ENG 90-4005, Urbana, IL, 1990.

[13] Gruber, M. R., Messersmith, N. L., and Dutton, J. C., "Three-Dimensional Velocity Field in a Compressible Mixing Layers," *AIAA Journal*, Vol. 31, No. 11, 1993, pp. 2039–2046.

[14] Clemens, N. T., and Mungal, M. G., "Two- and Three-Dimensional Effects in the Supersonic Mixing Layers," *AIAA Journal*, Vol. 30, No. 4, 1992, pp. 973–981.

[15] Hedges, L. S., and Eberhardt, D. S., "Comparison of Confined, Compressible, Spatially Developing Mixing Layers with Temporal Mixing Layers," *AIAA Journal*, Vol. 31, No. 11, 1993, pp. 1977–1983.

[16] Chien, K.-Y., Ferguson, R. E., Glaz, H. M., and Colella, P., "Inviscid Dynamics of Two-Dimensional Shear Layers," AIAA Paper 91-1678, June 1991.

[17] Lele, S. K., "Direct Numerical Simulation of Compressible Free Shear Flows," AIAA Paper 89-0374, Jan. 1989.

[18] Boris, J. P., Oran, E. S., Gardner, J. H., Kailasanath, K., and Young, T. R., Jr., "Computational Studies of a Localized Supersonic Shear Layer," AIAA Paper 89-0125, Jan. 1989.

[19] Sandham, N., and Reynolds, W. C., "The Compressible Mixing Layer: Linear Theory and Direct Simulation," AIAA Paper 89-0371, Jan. 1989.

[20] Leep, L. J., Dutton, J. C., and Burr, R. F., "Three-Dimensional Simulations of Compressible Mixing Layers: Visualizations and Statistical Analysis," *AIAA Journal*, Vol. 31, No. 11, 1993, pp. 2039–2046.

[21] Oh, C. K., "Very Large Eddy Simulations of Spatially Evolving Supersonic Turbulent Shear Layers," Ph.D. Thesis, Dept. of Aeronautical and Astronautical Engineering, Univ. of Illinois at Urbana–Champaign, Urbana, IL, Nov. 1993.

[22] Germano, M., Piomelli, U., Moin, P., and Cabot, W., "A Dynamic Subgrid-Scale Eddy Viscosity Model," *Physics of Fluids A*, Vol. 3, No. 7, 1991, pp. 1760–1765.

[23] Reynolds, W. C., "The Potential and Limitations of Direct and Large Eddy Simulations," *Lecture Notes in Physics*, edited by J. L. Lumley, Vol. 357, Springer-Verlag, Berlin, 1990, pp. 313–342.

[24] Ragab, S. A., Sheen, S.-C., and Sreedhar, M., "An Investigation of Finite-Difference Methods for Large Eddy Simulation of a Mixing Layer," AIAA Paper 92-0544, Jan. 1992.

[25] Boris, J. P., Grinstein, F. F., Oran, E. S., and Kolbe, R. L., "New Insight into Large Eddy Simulation," *Fluid Dynamics Research*, Vol. 10, 1992, pp. 199–228.

[26] Burr, R. F., and Dutton, J. C., "Numerical Simulations of Compressible and Reacting Temporal Mixing Layers and Implications for Modeling," AIAA Paper 91-1718, June 1991.

[27] Löhner, R., Morgan, K., Peraire, J., and Vahdati, M., "Finite Element Flux Corrected Transport (FEM-FCT) for the Euler and Navier–Stokes Equations," *International Journal for Numerical Methods in Fluids*, Vol. 7, No. 10, 1987, pp. 1093–1109.

[28] Wygnanski, I., and Fiedler, H., "The Two-Dimensional Mixing Region," *Journal of Fluid Mechanics*, Vol. 41, Dec. 1970, pp. 327–361.

[29] Koochesfahani, M. M., and Dimotakis, P. E., "Effects of a Downstream Disturbance on the Structure of a Turbulent Plane Mixing Layer," *AIAA Journal*, Vol. 27, No. 2, 1989, pp. 161–166.

[30] Messersmith, N. L., "An Experimental Investigation of Organized Structure and Mixing in Compressible Turbulent Free Shear Layers," Ph.D. Thesis, Dept. of Mechanical and Industrial Engineering, Univ. of Illinois at Urbana-Champaign, Urbana, IL, Jan. 1992.

[31] Puskas, E., DeAngelis, B., Oh, C. K., and Loth, E., "Vortex Tracking of a Supersonic Mixing Layer," Dept. of Aeronautical and Astronautical Engineering, Univ. of Illinois at Urbana-Champaign, Technical Rept. UILU ENG 93-0514, Urbana, IL, 1993.

[32] Lowery, P. S., and Reynolds, W. C., "Numerical Simulation of a Spatially-Developing, Forced, Plane Mixing Layer," Dept. of Mechanical Engineering, Stanford Univ., Rept. TF-26, Stanford, CA, 1986.

[33] Moser, R. D., and Rogers, M. M., "The Three-Dimensional Evolution of a Plane Mixing Layer: Pairing and Transition to Turbulence," *Journal of Fluid Mechanics*, Vol. 247, Feb. 1993, pp. 275–320.

[34] Samimy, M., and Elliot, G. S., "Effects of Compressibility on the Characteristics of Free Shear Layers," *AIAA Journal*, Vol. 28, No. 3, 1990, pp. 439–445.

[35] Koochesfahani, M. M., and Dimotakis, P. E., "Laser-Induced Fluorescence Measurements of Mixed Fluid Concentration in a Liquid Plane Mixing Layer," *AIAA Journal*, Vol. 23, No. 11, 1985, pp. 1700–1707.

[36] Fiedler, H. E., "Transport of Heat Across a Plane Turbulent Mixing Layer," *Advances in Geophysics*, edited by H. E. Landsberg and J. van Mieghem, Vol. 18A, Academic, New York, 1974, pp. 93–109.

[37] Sandham, N., and Reynolds, W. C., "Some Inlet-Plane Effects on the Numerically Simulated Spatially-Developing Mixing Layer," *Turbulent Shear Flows 6*, edited by J.-C. André, J. Cousteix, F. Durst, B. E. Launder, F. W. Schmidt, and J. H. Whitelaw, Springer-Verlag, New York, 1989, pp. 441–454.